IMPLEMENTING THE FAST MULTIPOLE BOUNDARY ELEMENT METHOD WITH HIGH-ORDER ELEMENTS

A. Gee*, B. Erdelyi†
Physics Dept., Northern Illinois University, DeKalb, IL 60115, USA

Abstract

The next generation of beam applications will require high-intensity beams with unprecedented control. For the new system designs, simulations that model collective effects must achieve greater accuracies and scales than conventional methods allow. The fast multipole method is a strong candidate for modeling collective effects due to its linear scaling. It is well known the boundary effects become important for such intense beams. We implemented a constant element fast boundary element method (FMBEM) [2] as our first step in studying the boundary effects. To reduce the number of elements and discretization error, our next step is to allow for curvilinear elements. In this paper, we will present our study on a quadratic and a cubic parametric method to model the surface.

INTRODUCTION

Beam applications have grown in the last few decades as has the need for precise control, particularly for high-intensity beams. However, collective and boundary effects become significant at such intensities. Conventional lattices are insufficient to prevent undesirable behavior. To facilitate future lattice designs, simulation models such as N-body solvers are being developed for large scale problems. In particular, the fast multipole method (FMM) is a strong candidate as a N-body solver due to its $O(N)$ scaling.

It is well known effects due to the beam pipe become important for high-intensity beams. To include boundary conditions for complicated structures, the boundary element method (BEM) has shown excellent results in various fields. However, the dense system matrix of size M can lead to $O(M^3)$ scaling in the worst scenario. The FMM has been used to accelerate the BEM, improving the scaling significantly [1]. In previous work, we combined our FMM module with a constant element BEM [2]. However, our results suggested the accuracy is strongly limited by the discretization error from flat panel elements. Parametric curvilinear elements are expected to improve the accuracy and performance of the FMBEM. We evaluated an analytical quadratic patch [3] and a constructive cubic patch [4] which use unit normals.

THEORY

Our constant element BEM in [2] was implemented using the single layer potential formulation, which leads to an ill-conditioned system [1]. We chose to continue using the double layer potential and the single layer field for Dirichlet and Neumann type BC, respectively. Equations 1 and 2 give the discretized integral equations with $\frac{\partial G}{\partial n_y} \equiv \mathbf{n}(\mathbf{y}) \cdot \boldsymbol{\nabla}_{\mathbf{y}} G$.

$$\phi(\mathbf{x}_i) = \sum_{j=1}^{M} \int_{\Gamma_j} \frac{\partial G}{\partial n_y}(\mathbf{x}_i, \mathbf{y}_j)\eta(\mathbf{y}_j)\mathrm{d}\Gamma(\mathbf{y}) \tag{1}$$

$$\frac{\partial \phi}{\partial n_x}(\mathbf{x}_i) = \sum_{j=1}^{M} \int_{\Gamma_j} \frac{\partial G}{\partial n_x}(\mathbf{x}_i, \mathbf{y}_j)\sigma(\mathbf{y}_j)\mathrm{d}\Gamma(\mathbf{y}) \tag{2}$$

From Eqs. 1 and 2 and the parametric area element, $\left|\frac{\partial \mathbf{x}}{\partial u} \times \frac{\partial \mathbf{x}}{\partial v}\right|$, it is imperative our parametrization gives accurate normals on the element and interpolates the normals at the vertices for continuity. We decided on two methods given in [3] and [4].

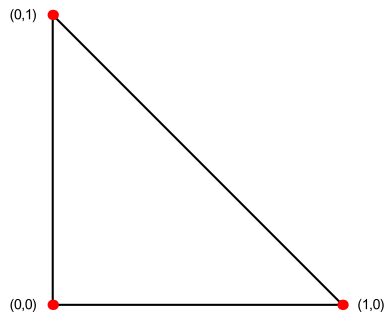

Figure 1: Triangle in (u, v) with vertices $\mathbf{x}_1 = \mathbf{x}(0,0)$, $\mathbf{x}_2 = \mathbf{x}(1,0)$, $\mathbf{x}_3 = \mathbf{x}(0,1)$ and corresponding normals.

The quadratic patch in [3] fits an order 2 polynomial of form $\mathbf{x}(u,v) = \mathbf{a}_{00} + \mathbf{a}_{10}u + \mathbf{a}_{01}v + \mathbf{a}_{20}u^2 + \mathbf{a}_{11}uv + \mathbf{a}_{02}v^2$ given vertices $\mathbf{x}_1, \mathbf{x}_2, \mathbf{x}_3$ and normals $\mathbf{n}_1, \mathbf{n}_2, \mathbf{n}_3$. For a triangle as in Fig. 1, the coefficients are given in Eq. 3. $\mathbf{c}(\mathbf{d}_{ij}, \mathbf{n}_i, \mathbf{n}_j)$ in Eq. 3 is termed the curvature parameter in [3] and can be calculated by Eq. 4. [3] gives details on the derivation.

$$\begin{aligned} \mathbf{d}_{ij} &\equiv \mathbf{x}_j - \mathbf{x}_i \\ \mathbf{c}_{ij} &\equiv \mathbf{c}(\mathbf{d}_{ij}, \mathbf{n}_i, \mathbf{n}_j) \\ \mathbf{a}_{00} &= \mathbf{x}_1 & \mathbf{a}_{20} &= \mathbf{c}_{12} \\ \mathbf{a}_{10} &= \mathbf{d}_{12} - \mathbf{c}_{12} & \mathbf{a}_{11} &= \mathbf{c}_{12} + \mathbf{c}_{13} - \mathbf{c}_{23} \\ \mathbf{a}_{01} &= \mathbf{d}_{13} - \mathbf{c}_{13} & \mathbf{a}_{02} &= \mathbf{c}_{23} \end{aligned} \tag{3}$$

$$\begin{aligned} \boldsymbol{\nu} &= \frac{\mathbf{n}_i + \mathbf{n}_j}{2} & d &= \mathbf{d}_{ij} \cdot \boldsymbol{\nu} & c &= 1 - 2\Delta c \\ \Delta\boldsymbol{\nu} &= \frac{\mathbf{n}_i - \mathbf{n}_j}{2} & \Delta d &= \mathbf{d}_{ij} \cdot \Delta\boldsymbol{\nu} & \Delta c &= \mathbf{n}_i \cdot \Delta\boldsymbol{\nu} \end{aligned}$$

$$\mathbf{c}(\mathbf{d}_{ij}, \mathbf{n}_i, \mathbf{n}_j) = \begin{cases} \frac{\Delta d}{1 - \Delta c}\boldsymbol{\nu} + \frac{d}{\Delta c}\Delta\boldsymbol{\nu} & c \neq \pm 1 \\ \mathbf{0} & c = \pm 1 \end{cases} \tag{4}$$

* agee1@niu.edu
† berdelyi@niu.edu

The cubic patch in [4] constructs a surface using order 3 polynomials by separately fitting over two edges sharing a vertex and spanning a third curve across the patch. In [4], this was purely constructive to calculate 10 points on the patch and fit using Lagrange interpolation. However, we wished to examine the constructed polynomials as an analytical surface. The coefficients for the univariate cubic polynomial, $\mathbf{p}(u) = \mathbf{a}_0 + \mathbf{a}_1 u + \mathbf{a}_2 u^2 + \mathbf{a}_3 u^3$, are given in Equation 5.

$$\alpha = \frac{(\mathbf{x}_2 - \mathbf{x}_1) \cdot \left[(\mathbf{n}_2 \cdot \mathbf{n}_2)\mathbf{n}_1 + \frac{1}{2}(\mathbf{n}_1 \cdot \mathbf{n}_2)\mathbf{n}_2\right]}{\frac{2}{3}(\mathbf{n}_1 \cdot \mathbf{n}_1)(\mathbf{n}_2 \cdot \mathbf{n}_2) - \frac{1}{6}(\mathbf{n}_1 \cdot \mathbf{n}_2)}$$

$$\beta = \frac{-(\mathbf{x}_2 - \mathbf{x}_1) \cdot \mathbf{n}_2 - \frac{1}{3}(\mathbf{n}_1 \cdot \mathbf{n}_2)\alpha}{\frac{2}{3}(\mathbf{n}_2 \cdot \mathbf{n}_2)}$$

$$\begin{aligned} \mathbf{a}_0 &= \mathbf{x}_1 & \mathbf{a}_2 &= \alpha \mathbf{n}_1 \\ \mathbf{a}_1 &= \mathbf{x}_2 - \mathbf{a}_0 - \mathbf{a}_2 - \mathbf{a}_3 & \mathbf{a}_3 &= \frac{1}{3}(\beta \mathbf{n}_2 - \mathbf{a}_2) \end{aligned} \tag{5}$$

$$\mathbf{k}(u) = \frac{1}{\left|\frac{d\mathbf{p}}{du}\right|^2}\left[\frac{d^2\mathbf{p}}{du^2} - \frac{\frac{d\mathbf{p}}{du} \cdot \frac{d^2\mathbf{p}}{du^2}}{\left|\frac{d\mathbf{p}}{du}\right|^2}\frac{d\mathbf{p}}{du}\right] \tag{6}$$

As in [4], we construct $\mathbf{p}_{12}(u)$ and $\mathbf{p}_{13}(u)$ and their normals $\mathbf{k}_{12}(u)$ and $\mathbf{k}_{13}(u)$ using Eq. 6, where ij refers to the edge between vertices i and j. We then construct the spanning curve, $\mathbf{x}(u, v) = \mathbf{a}_0(u) + \mathbf{a}_1(u)v + \mathbf{a}_2(u)v^2 + \mathbf{a}_3(u)v^3$, where $\mathbf{x}_1 \rightarrow \mathbf{p}_{12}, \mathbf{x}_2 \rightarrow \mathbf{p}_{13}, \mathbf{n}_1 \rightarrow \mathbf{k}_{12}, \mathbf{n}_2 \rightarrow \mathbf{k}_{13}$, which ultimately gives a bivariate cubic with $(u, v) \in [0, 1] \times [0, 1]$ over the entire patch. This is mapped to the triangle in Fig. 1 as described by [4]. Normalization is only needed at the end.

In [4], they impose the approximation, $\frac{d^2\mathbf{x}}{du^2} \parallel \mathbf{n}$ at the endpoints. The effect of this approximation is unclear. The constructed cubic polynomial $\mathbf{x}$(u,v) [4] is cumbersome in practice. We also evaluate the 3rd order Taylor expansion of $\mathbf{x}(u, v)$ and corresponding normal for actual use.

ANALYSIS

The previous methods were implemented and tested using a spherical triangle and a flat panel discretized sphere. The centroids, unit normals and areas are easily computed and provide a simple test in addition to testing the interpolation conditions. The area element is tested by $\iint \left|\frac{\partial \mathbf{x}}{\partial u} \times \frac{\partial \mathbf{x}}{\partial v}\right| du dv$.

The spherical triangle is formed by picking 3 points in the first octant of a sphere centered at $(0, 0, 0)$ with radius R and forming the corresponding spherical arcs. This prevents an angle $> \frac{\pi}{2}$ between the normals. The spherical triangle area is given by $R^2(A + B + C - \pi)$ where A, B, C are the interior angles and can be found in numerous ways. The parameters for the spherical triangle are given in Table 1 and chosen for a relatively large area to amplify the errors.

We represent the spherical triangle (green) in Fig. 2. The quadratic patch showed good results for this case. Figure 2a shows the patch (blue) has a slight deviation in the center but represents the shape well. In Fig. 2b, the constructed polynomial (blue) shows significant deviation around the center but interpolates the vertices correctly. However, its 3rd order Taylor expansion (red) deviates significantly and does not interpolate $\mathbf{x}_3$ at all.

Table 1: Spherical Triangle Parameters

Vertices	(8.93, 4.49, 0.27) (3.08, 6.60, 6.85) (8.63, 0.54, 5.02)
Center	(7.75, 4.37, 4.56)
Radius	10
Area	28.970

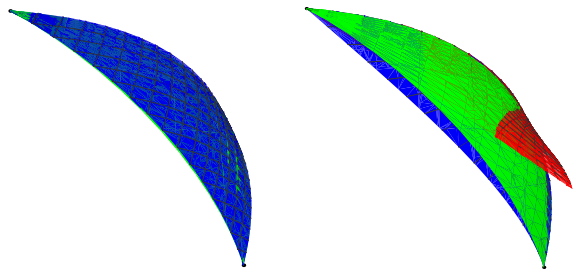

(a) Quadratic patch (blue) (b) Cubic patch (blue) and truncated cubic (red)

Figure 2: Comparison of parametric patches on the spherical triangle (green) given by Table 1. In Figure 2a, the quadratic patch (blue) deviates slightly in the center. In Figure 2b, the patch using a cubic polynomial (blue) vs its 3rd order Taylor expansion (red) deviate significantly in this case.

We evaluated the centroid and unit normal at $(1/3, 1/3)$ for the quadratic patch and equivalently $(2/3, 1/2)$ for the cubic patch mapped from Fig. 1. The percent errors are given in Table 2. We show the L_2-norm in the case of the centroid and unit normal. The results suggest the truncation of the Taylor expansion affected the area element significantly. Since the parametric surface does not match, the error in the unit normal for the truncated cubic is inconclusive.

Table 2: Percent Errors On Spherical Triangle

	Centroid	Normal	Area
Quadratic	0.79	0.44	-0.33
Cubic	1.63	6.49	1.53
Truncated cubic	4.19	30.5	13.6

The previous results reflect the case of a large element. To check with practical elements, we chose a sphere discretized by flat panels or constant elements, where we know the vertices and normals lie on the surface. In this case, only the 3rd order Taylor expansion could be evaluated for the cubic patch. Following the same analysis, we checked the area, centroid and unit normals for each element after verifying similar behavior at vertices as before.

Figure 3 shows the standard deviation in the difference of the x-component for the centroid and its unit normal from the quadratic and cubic patch versus the number of elements. This was approximately the same for x, y, z. We can see the range of the difference in the centroid shrinks rapidly for the quadratic patch but flattens out early for the cubic patch. Figure 4 shows similar behavior for the percent error

in the area of the sphere. The percent error in area for the truncated cubic is approximately the same as for the flat panel discretization. The results suggest the truncated cubic patch will not give an adequate representation of the structure even with a practical element size. There is an essential interpolation property lost in the higher order terms. We will need to revisit the derivation in [4].

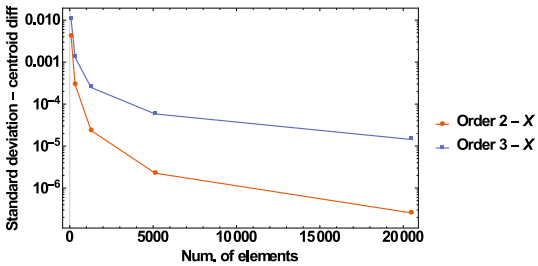

(a) Centroid vs. number of elements

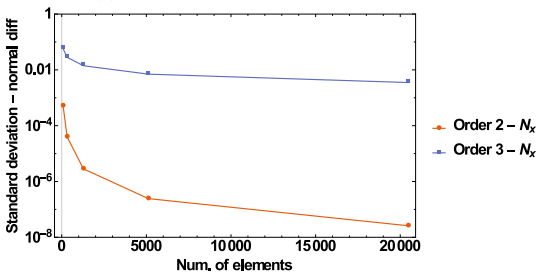

(b) Unit normal vs. number of elements

Figure 3: Standard deviation in the difference of (3a) the centroid and (3b) the unit normal. The error bound for the quadratic patch quickly shrinks until $M \sim 5000$.

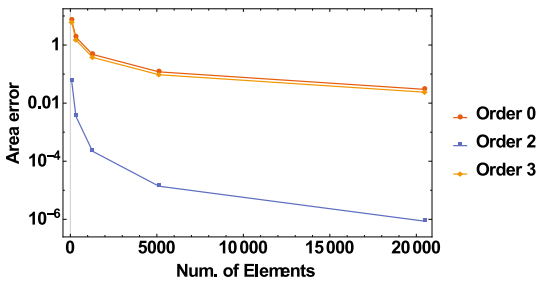

Figure 4: Percent error in the area vs no. of elements for the flat panel, quadratic, and truncated cubic parametrization. The truncated cubic gives essentially the same error as the flat panel discretization.

We next examine the runtime in Fig. 5. Figure 5a shows the overall runtime and Fig. 5b shows the runtime separated by construction of the parametric function and the area integration for the quadratic and cubic patches. For the flat panel element, there is essentially no distinction. Figure 5a shows the runtime increases significantly with number of elements. Figure 5b shows the integration essentially dominates when $M > 1000$, which results in the increase. Due to this, the runtime for the quadratic and cubic patches are similar.

CONCLUSION

We evaluated the quadratic parametric patch in [3] and the cubic patch in [4] as options for higher order discretization. Because we chose the well-conditioned double layer potential and single layer field integral equations, it is essential to accurately describe the normals across the structure's surface. We showed the quadratic patch gives adequate accuracy for large elements or small M. However, the truncated cubic patch needs to be studied further. We lose an essential interpolation property in the higher order terms, greatly reducing the patch quality. The runtime is mainly dominated by the integration, which we may improve using differential algebraic methods. Our next steps will be to allow for discontinuities such as edges or corners and decide whether element order > 3 will be necessary for our purposes.

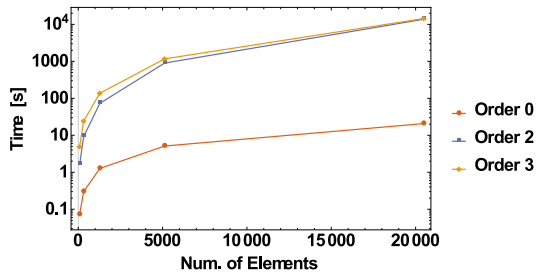

(a) Overall runtime

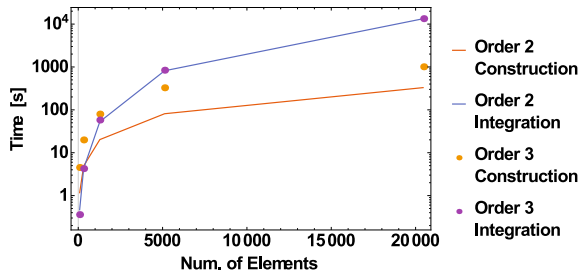

(b) Construction vs integration runtime

Figure 5: Runtime comparison between the different methods. Overall, quadratic and cubic are similar due to the integration step.

ACKNOWLEDGMENT

This work was supported in part by the U.S. Department of Energy, Office of High Energy Physics, under Contract No. DE-SC0011831 with Northern Illinois University.

REFERENCES

[1] Yijun Liu, Fast Multipole Boundary Element Method: Theory and Applications in Engineering, Cambridge, MA, USA: Cambridge University Press, 2009.

[2] A. Gee and B. Erdelyi, "A differential algebraic framework for the fast indirect boundary element method," in *Proc. IPAC'16*, Busan, South Korea, May 2016, pp.3107-3109.

[3] Nagata, Takashi. "Simple local interpolation of surfaces using normal vectors." Comp. Aided Geom. Design vol. 22, pp. 327-347, 2005.

[4] Geng, Weihua. "Parallel higher-order boundary integral electrostatics computation on molecular surfaces with curved triangulation." Journal Comp. Phys. vol. 241, pp. 253-265, 2013.